Gradient and nongradient contributions to plasmon-enhanced optical forces on silver nanoparticles

Vance Wong and Mark A. Ratner
Center for Nanofabrication and Molecular Self-Assembly, Department of Chemistry, Northwestern University, Evanston, Illinois 60208, USA

(Received 9 September 2005; revised manuscript received 14 December 2005; published 10 February 2006)

We use a computational method based on the discrete-dipole approximation (DDA) to calculate the gradient and nongradient contributions to optical forces on nanometer sized silver particles in water. We find that, due to a contribution that is usually neglected, nongradient forces are often non-negligible. This result is not a consequence of an approach to the dipole limit. We suggest that this method could provide useful input for a more detailed understanding of the physics relevant to optical trapping and binding phenomena.

DOI: 10.1103/PhysRevB.73.075416 PACS number(s): 78.67.Bf, 41.20.−q, 78.20.−e

I. INTRODUCTION

Exploitation of optical forces to trap and manipulate mesoscopic matter has taken many forms. Experiments have successfully demonstrated the potential to provide an impressive level of noninvasive control with applications to, among other areas, nanofabrication,[1,2] biomolecular mechanics,[3] and microfluidics-based biological assay technology.[4] Proposed applications seem to be equally numerous and include optical force microscopy[5] and spectroscopy,[6] single molecule Raman spectroscopy,[7,8] and nanoparticle organization.[9]

Theoretical approaches to these phenomena have often focused on the importance of the gradient force as the dominant contribution to the total force.[7,10–12] In the following, we use a numerical method to compute explicitly the gradient and nongradient contributions to the total optically induced force on uncharged metallic particles in an external field. We find that, due to a contribution that is typically neglected, nongradient forces are often comparable to the gradient contribution. The results discussed in Ref. 17 show that this is not a consequence of an approach to the dipole limit for small particles. This suggests the need for a more thorough examination of the basic physics relevant to optical trapping and its many applications.

II. THEORY AND NUMERICAL APPROACH

The time-averaged force on a dipole in a harmonic electromagnetic field (neglecting a term due to the particle motion[13]) can be written as,

$$\langle \mathbf{F} \rangle = \frac{1}{4}\mathrm{Re}(\alpha)\boldsymbol{\nabla}|\mathbf{E}|^2 + \frac{k}{2}\mathrm{Im}(\alpha)\mathrm{Re}(\mathbf{E}^* \times \mathbf{B}) + \frac{1}{2}\mathrm{Im}(\alpha)\mathrm{Im}[(\mathbf{E}^* \cdot \boldsymbol{\nabla})\mathbf{E}]. \quad (1)$$

A derivation is given elsewhere.[14] It is assumed for convenience that the complex polarizability α is a scalar and $k = \omega/c$. A nearly identical expression has appeared in the literature recently.[15,16] The first term is the gradient force. The second term is the dissipative radiation-pressure force. The last term is not explicitly named in the literature. It is worth noting that, in the scenario depicted in Fig. 1(b), the gradient force acting on one of the particles is not conservative in the event that the other particle is permitted to move. The work done by the gradient force on a particle undergoing closed-loop motion does not necessarily vanish if the other particle is also in motion. Therefore, the interaction is not describable by a scalar potential, even if the gradient contribution is much larger than the others. In a single particle experiment, or in the event that one of the particles is fixed (e.g., a stationary scanning probe tip), the gradient force on the moving

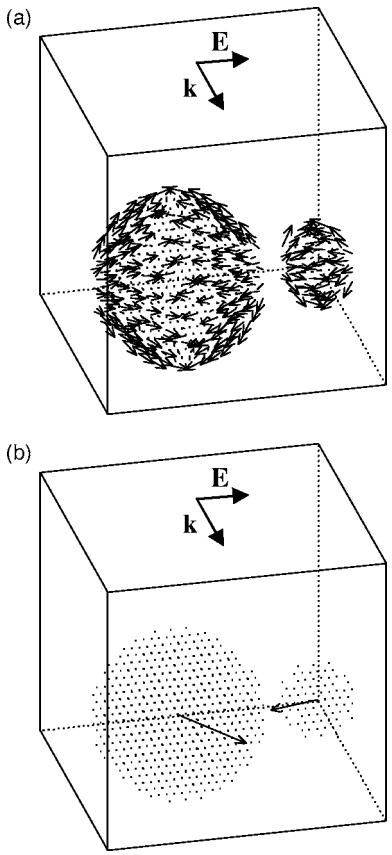

FIG. 1. Illustration of the use of Eq. (1) to compute total forces on particles. Forces on individual dipoles depicted in (a) are summed to give the resultant forces on each sphere shown in (b).

particle is conservative, and Eq. (1) does provide a decomposition of the force into its conservative and nonconservative contributions. The applicability of a scalar potential in the case of nanoscale particles is often justified by appealing to a size scaling argument.[10–12] The size scaling of each of the contributions in Eq. (1) is explored elsewhere.[17]

We now turn our attention to three previously published expressions for the total optical force on a dipole in an electromagnetic field.[15,16,18,19] The main reason for doing this is to show that our method provides a unified framework for studying gradient and nongradient contributions to the total force. To this end, we show that the three formulations are equivalent. We begin with an expression for the negative gradient of the classical dipole-field interaction Hamiltonian,[18,20]

$$\langle \mathbf{F} \rangle = \frac{1}{2} \sum_i \mathbf{e}_i \sum_j \mathrm{Re}\left[\alpha \mathbf{E}_j \left(\frac{\partial \mathbf{E}_j}{\partial x_i} \right)^* \right]. \tag{2}$$

Here, i and j indicate the Cartesian components or coordinates ($\mathbf{e}_i$ are Cartesian unit vectors). Equation (2) has been used as the basis for numerical studies of optical trapping by evanescent waves at the surface of a refractive medium,[21] optical binding of dielectric and absorbing spheres in an external field,[12] and photonic force spectroscopy.[6] As suggested in Ref. 18, Eq. (2) may be rewritten as

$$\langle \mathbf{F} \rangle = \frac{1}{2} \sum_i \mathbf{e}_i \, \mathrm{Re}\left\{ [\mathrm{Re}(\alpha) + i \, \mathrm{Im}(\alpha)] \mathbf{E} \cdot \left(\frac{\partial \mathbf{E}}{\partial x_i} \right)^* \right\} \tag{3}$$

$$= \frac{1}{2} \sum_i \mathbf{e}_i \, \mathrm{Re}(\alpha) \mathrm{Re}\left[\mathbf{E} \cdot \left(\frac{\partial \mathbf{E}}{\partial x_i} \right)^* \right] - \frac{1}{2} \sum_i \mathbf{e}_i \, \mathrm{Im}(\alpha) \mathrm{Im}\left[\mathbf{E} \cdot \left(\frac{\partial \mathbf{E}}{\partial x_i} \right)^* \right]. \tag{4}$$

Using

$$\frac{\partial}{\partial x_i} (\mathbf{E}^* \cdot \mathbf{E}) = 2 \, \mathrm{Re}\left[\mathbf{E} \cdot \left(\frac{\partial \mathbf{E}}{\partial x_i} \right)^* \right], \tag{5}$$

we finally arrive at

$$\langle \mathbf{F} \rangle = \frac{1}{4} \sum_i \mathbf{e}_i \, \mathrm{Re}(\alpha) \frac{\partial}{\partial x_i} |\mathbf{E}|^2 + \frac{1}{2} \sum_i \mathbf{e}_i \, \mathrm{Im}(\alpha) \mathrm{Im}\left[\mathbf{E}^* \cdot \left(\frac{\partial \mathbf{E}}{\partial x_i} \right) \right]. \tag{6}$$

This expression has been published previously.[18] The first term is the gradient force, and the second is the scattering force. We can show that the second and third terms in Eq. (1) sum to give the scattering force. Using Faraday's law and the harmonic time dependence of the fields to recast the radiation-pressure term, we have

$$\frac{k}{2} \mathrm{Im}(\alpha) \, \mathrm{Re}(\mathbf{E}^* \times \mathbf{B}) = \frac{\mathrm{Im}(\alpha)}{2} \, \mathrm{Im}(\mathbf{E}^* \times \boldsymbol{\nabla} \times \mathbf{E}). \tag{7}$$

Summing this with the third term in Eq. (1) gives,

$$\mathbf{F}_{rad-press} + \mathbf{F}_{(\mathbf{E}^* \cdot \boldsymbol{\nabla}) \mathbf{E}} = \frac{\mathrm{Im}(\alpha)}{2} \, \mathrm{Im}[(\mathbf{E}^* \times \boldsymbol{\nabla} \times \mathbf{E}) + (\mathbf{E}^* \cdot \boldsymbol{\nabla}) \mathbf{E}]. \tag{8}$$

An elementary vector identity[22] shows that

$$\mathbf{E}^* \times \boldsymbol{\nabla} \times \mathbf{E} + (\mathbf{E}^* \cdot \boldsymbol{\nabla}) \mathbf{E} = \sum_i \mathbf{e}_i \left(\mathbf{E}^* \cdot \frac{\partial \mathbf{E}}{\partial x_i} \right). \tag{9}$$

Combining Eqs. (8) and (9) gives

$$\mathbf{F}_{rad-press} + \mathbf{F}_{(\mathbf{E}^* \cdot \boldsymbol{\nabla}) \mathbf{E}} = \frac{\mathrm{Im}(\alpha)}{2} \sum_i \mathbf{e}_i \, \mathrm{Im}\left(\mathbf{E}^* \cdot \frac{\partial \mathbf{E}}{\partial x_i} \right). \tag{10}$$

Comparing Eq. (10) with Eq. (6), we see that the scattering force can be decomposed into the sum of the radiation-pressure term and the unnamed third term in Eq. (1). Equations (1), (2), and (6) are equivalent expressions for the force, so Eq. (1) provides a unified framework for analyzing the nongradient components, which are usually dealt with by other means, as mentioned earlier. In Ref. 15, a decomposition of the force on a nanoparticle (treated as a point dipole) under nonplane wave illumination was performed. Reference 17 discusses some ramifications choosing a point dipole description of a mesoscopic particle.

To evaluate all three terms in Eq. (1), self-consistent optical scattering equations are solved in the discrete-dipole approximation (DDA)[23] using a publicly available code.[24] Then, using a fast Fourier transform-based scheme, each term is explicitly computed for every dipole used to represent the target particles.[14] The approach is based on a previously developed method for computing the total force on individual dipoles in a DDA calculation.[25] The forces are then summed over the set of dipoles comprising different particles to find the net forces on each particle. Figure 1 illustrates the procedure. In Fig. 1(a), the force on each dipole in the large sphere can be summed to approximate the total force on the entire sphere, and the same can be done for the small sphere. The resultant forces are depicted in Fig. 1(b). In the case studies below, the targets are composed of two silver particles immersed in water, and plane wave excitation is assumed. The effect of water on the optical response is accounted for using a modified dielectric constant for the particle.[24] The larger particle is roughly 100 times the volume of the smaller particle. We chose to model a size asymmetric target because this is the situation typically encountered in experiments demonstrating photoinduced formation of silver nanoprisms.[26–28] Damping and broadening, known to occur in small particles due to surface scattering[29] and nonlocal dielectric effects,[30] are neglected. Local field corrections[31–33] are also ignored since the main objective is to determine the relative sizes of the three terms in Eq. (1) under different conditions. The computations on larger particles than those considered below yielded comparable results.

III. RESULTS AND DISCUSSION

A naïve appeal to Eq. (1) suggests that the gradient force could dominate at wavelengths where $\mathrm{Re}(\alpha) \gg \mathrm{Im}(\alpha)$. How-

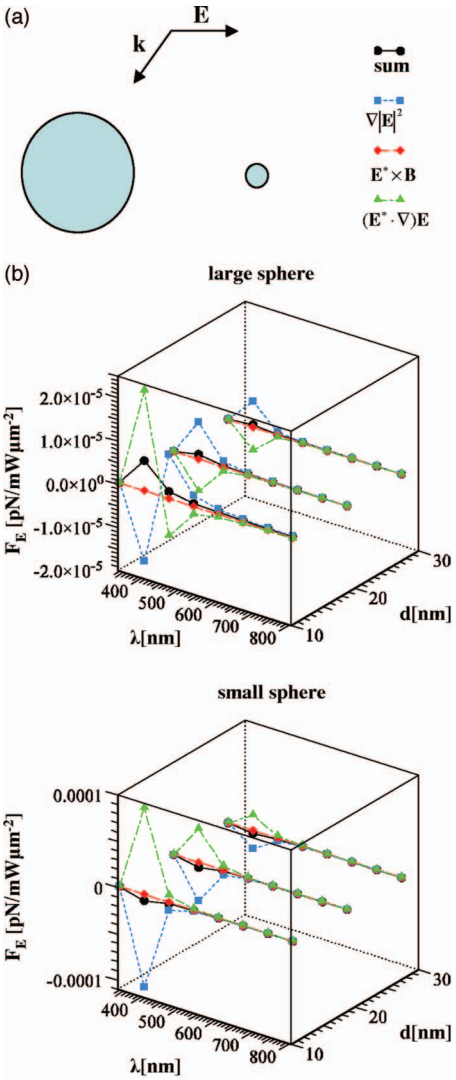

FIG. 2. (Color) Total force and contributions for a two sphere target. The spheres have radii of $A=5$ nm and $a=1.08$ nm. (a) The target and field geometry with key for (b). (b) Decomposition of forces along $\mathbf{E}$ for both spheres as a function of wavelength and distance. Forces on the large sphere have been multiplied by $M=1,2,5$ at $d=10.3$, 18.9, and 27.4 nm, respectively. Small sphere multiplication factors are $m=1,10,25$.

ever, inspection of the force spectra for particles represented by many dipoles reveals a more complicated relationship among the three terms in Eq. (1). The relative contributions of the three terms depend on target geometry (e.g., particle shape, relative position, and orientation) as well as external field parameters (e.g., wavelength, incident direction, and polarization). Also, whereas absorption and scattering spectra (not shown) were found to be quite insensitive to variations in some of these parameters (e.g., relative orientation of particles, interparticle distance), net forces and their contributions displayed a nontrivial dependence on them.

Fig. 2 shows the results of force calculations on a two-sphere target. The target-field geometry is shown in Fig. 2(a). Figure 2(b) shows contributions to the total force on the large and small spheres. Evidently, the $(\mathbf{E}^*\cdot\nabla)\mathbf{E}$ force is comparable to the gradient force over nearly the entire spectrum, and for all intersphere separations examined. The radiation-pressure contribution is negligible as argued elsewhere.[7,10–12] The two non-negligible terms generally have opposite signs. The net force is thereby determined by the approximate cancellation of two terms whose sizes are greater than the size of the resultant force. We found this to be a surprisingly common, though not universal, feature of the force spectra, especially for spheres. Qualitative differences in the appearance of the force spectra can occur as a function of distance; note the sign changes in the gradient and $(\mathbf{E}^*\cdot\nabla)\mathbf{E}$ terms for the large sphere ($d=10.3$ nm). While the total forces along $\mathbf{E}$ on the two spheres are equal and opposite, the gradient and $(\mathbf{E}^*\cdot\nabla)\mathbf{E}$ forces are larger for the small sphere at small separations. The situation is reversed at large separations so the distance decay of these two terms is more rapid for the small sphere than for the large sphere. The distance-dependence of forces is not examined here in detail. However, the asymptotic decay of the total force has been predicted to be $\sim d^{-4}$, as would be expected from a dipole-dipole interaction.[9] In this geometry, the total forces on the two spheres result in an attractive interaction.

Figure 3 shows results for a large prolate ellipsoid (major to minor axis ratio, $R=3.2$) and a small sphere with the geometry as in Fig. 3(a). As in the previous example, gradient and $(\mathbf{E}^*\cdot\nabla)\mathbf{E}$ contributions are opposite in sign over almost the entire spectrum, for both prolate and sphere, and for all interparticle distances considered. For the prolate, they are usually of roughly equal magnitude. By contrast, for the sphere, the gradient term dominates to the red of the long wavelength resonance. The radiation-pressure component is negligible. Again, qualitative differences in the gradient and $(\mathbf{E}^*\cdot\nabla)\mathbf{E}$ force spectra occur as a function of the particle separation. At the shortest distance, neither contribution to the force on the prolate undergoes a sign change as a function of wavelength. As the interparticle separation increases, multiple crossovers in both occur. Long wavelength extrema decay more rapidly than short wavelength extrema with distance. The total force spectrum appearance changes far less than its contributions. For the sphere, one sign inversion occurs for the gradient and $(\mathbf{E}^*\cdot\nabla)\mathbf{E}$ contributions. As for the prolate, long wavelength extrema decay more rapidly than the short wavelength extrema. In contrast to the two sphere case, the net interaction is weakly repulsive at short wavelengths. Notice that the long wavelength tails of the gradient and net forces are attractive. This appears to be a generic feature when the field is parallel to the interparticle axis. By contrast, when the field is normal to this axis, the long wavelength tail is repulsive, though an attractive interaction may still appear at a resonance (see Fig. 4). The distance dependence of the gradient and $(\mathbf{E}^*\cdot\nabla)\mathbf{E}$ terms is much closer to being the same for the prolate and sphere than was the case for the two spheres.

The same prolate and sphere are considered in Fig. 4, but with a different orientation than in Fig. 3. We note that optical spectra (not shown) for this configuration are nearly

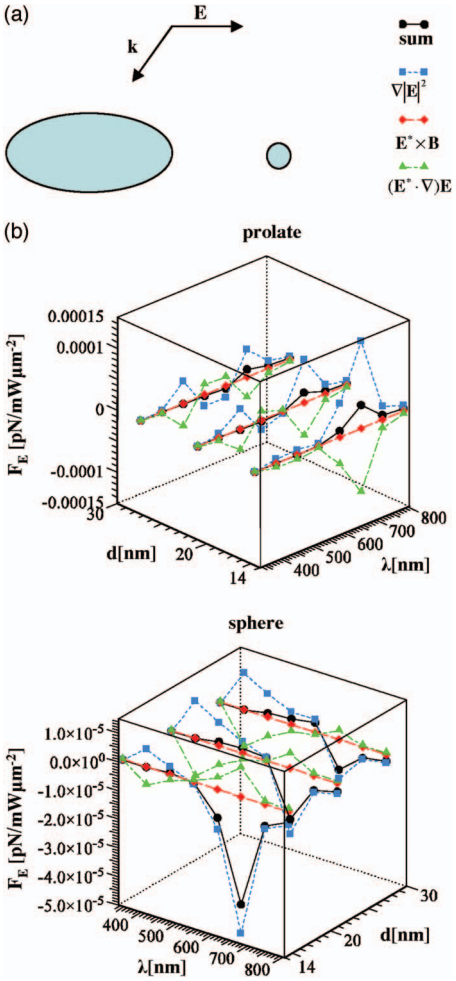

FIG. 3. (Color) Total force and contributions for a prolate and sphere. The prolate has an effective radius of (see Refs. 23 and 24) $A=5$ nm and the sphere $a=1.08$ nm. The prolate major to minor axis ratio is $R=3.2$. (a) The target and field geometry with key for (b). (b) Decomposition of forces along $\mathbf{E}$ for both particles as a function of wavelength and distance. Magnification factors for prolate and sphere are $M=1,15,50$ at $d=14.6$, 21.0, and 27.4 nm.

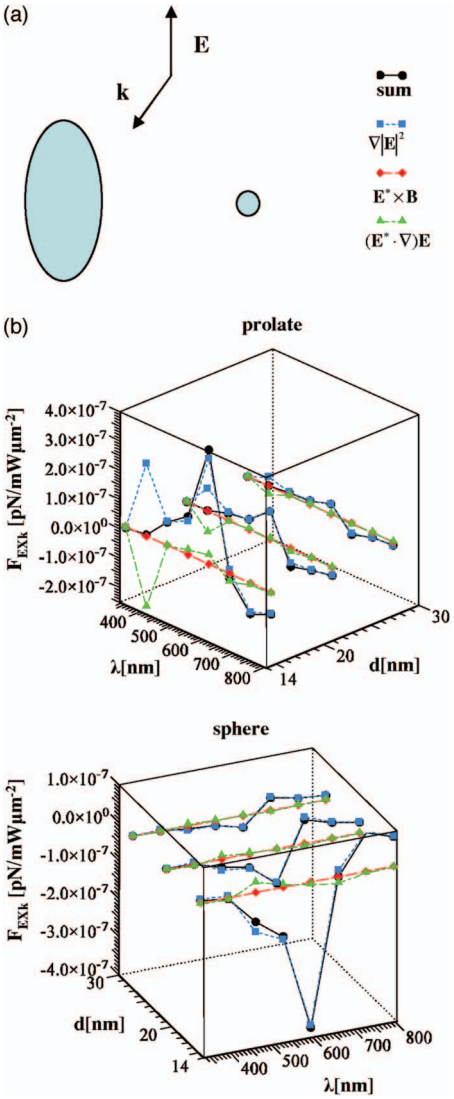

FIG. 4. (Color) Total force and contributions for prolate and sphere. (a) The target and field geometry with key for (b). Note the changes in the prolate-sphere orientation and polarization from Fig. 3. (b) Decomposition of forces along $\mathbf{E}\times\mathbf{k}$ for both particles as a function of wavelength and distance. $M=1$ (prolate and sphere) at $d=14.6$, 21.0, and 27.4 nm.

indistinguishable from those corresponding to Fig. 3. Far field properties are dominated by the prolate, which is 100 times larger than the sphere. However, there are clear differences in the force spectra. Total force peaks for this geometry are blue-shifted from Fig. 3, as well as being far weaker. As alluded to earlier, while there is an attractive resonance, the long wavelength tail is repulsive. The distance dependence is far weaker in this case, which is due in part to the much larger edge-to-edge distance despite having an equal center-of-mass to center-of-mass distance. In contrast to the previous example, for the prolate, the distance-dependent decay of the short wavelength resonance in gradient and $(\mathbf{E}^*\cdot\nabla)\mathbf{E}$ contributions is similar to that of the long wavelength resonance. Gradient and $(\mathbf{E}^*\cdot\nabla)\mathbf{E}$ terms also undergo a similar distance decay, leading to relatively invariant total-force spectra. For wavelengths to the red of 500 nm, the gradient contribution is substantially larger than the $(\mathbf{E}^*\cdot\nabla)\mathbf{E}$ term for both the prolate and sphere. Additional results with oblate and sphere geometries (not shown) suggest that this may be generic behavior in the near field.

When the target-field geometry is as shown in Fig. 5(a), the prolate total and gradient-force spectra appear essentially independent of particle separation, though there are subtle changes in the $(\mathbf{E}^*\cdot\nabla)\mathbf{E}$ contribution at short wavelengths. In contrast to the previous examples, radiation-pressure is no longer negligible for the sphere near its dipole resonance. The long wavelength oscillation in the total-force spectrum of the sphere closely follows the gradient contribution and decays faster with distance than short wavelength features. This is because the gradient contribution to the force on the sphere is strongly influenced by the prolate. For the sphere,

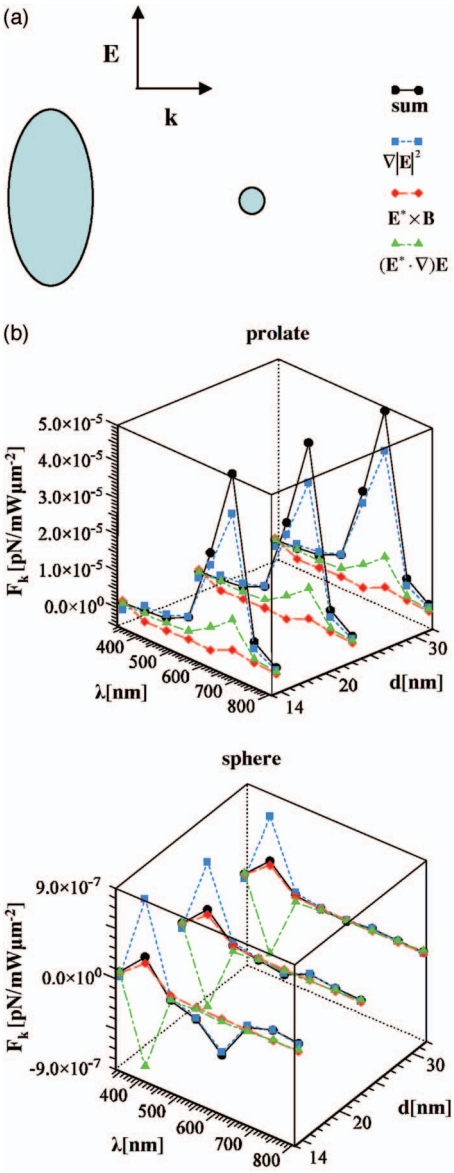

FIG. 5. (Color) Total force and contributions for prolate and sphere. (a) The target and field geometry with key for (b). Note the change in direction of incidence from Fig. 4. (b) Decomposition of forces along **k** for both particles as a function of wavelength and distance. $M=1$ (prolate and sphere) at $d=14.6$, 23.1, and 31.6 nm.

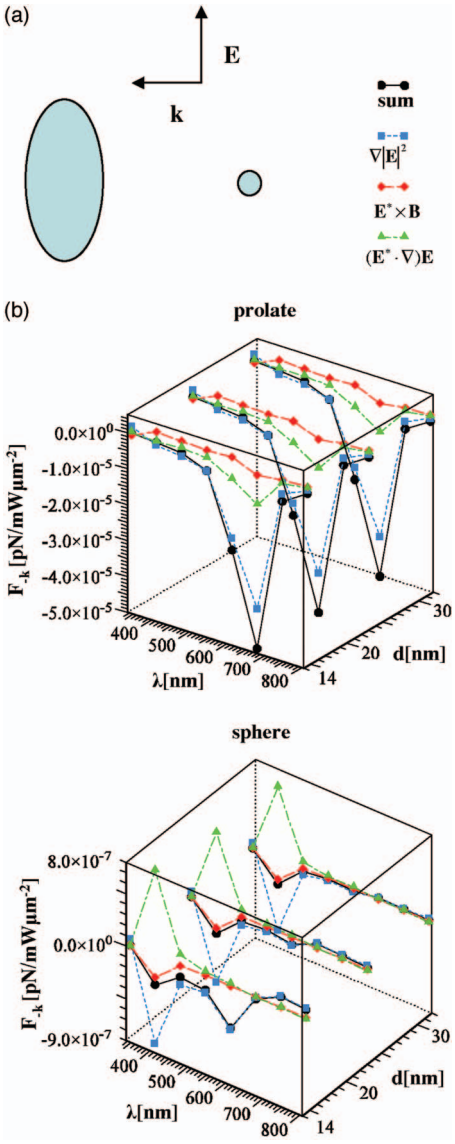

FIG. 6. (Color) Total force and contributions for prolate and sphere. (a) The target and field geometry with key for (b). Note the change in direction of incidence from Fig. 5. (b) Decomposition of forces along $-\mathbf{k}$ for both particles as a function of wavelength and distance. $M=1$ (prolate and sphere) at $d=14.6$, 23.1, and 31.6 nm.

the $(\mathbf{E}^*\cdot\nabla)\mathbf{E}$ term is relatively featureless in the long wavelength part of the spectrum. The long wavelength tails of the gradient and total forces are again repulsive. This is confirmed by transforming to the reduced mass-relative coordinate system (results not shown). Similar trends are evident when the incident wave vector is inverted (Fig. 6). Note that the signs of the gradient and $(\mathbf{E}^*\cdot\nabla)\mathbf{E}$ contributions are generally inverted from Fig. 5, except for the sphere at the long wavelength resonance. The coordinate transformation verifies that, at the long wavelength resonance, the interaction is now repulsive since the prolate is pushed away from the sphere.

IV. CONCLUSION

The numerical examples presented above show that the $(\mathbf{E}^*\cdot\nabla)\mathbf{E}$ contribution is frequently comparable to the gradient term in optical forces between the absorbing mesoscopic particles in plane wave incident fields. They also show that the total force on a particle can be determined by an intricate interplay among all three terms in Eq. (1), with highly nontrivial wavelength and distance dependencies. The implications for optical trapping scenarios involving nonplane wave incident fields can be explored with minor modifications to the numerical method.[14] A comprehensive theoretical treatment of these phenomena has yet to be achieved. The computational method demonstrated above promises to provide detailed information that could be useful in the development of such an understanding.

ACKNOWLEDGMENTS

We thank Professor George Schatz and Dr. Shengli Zou for enlightening discussions and assistance with the public DDA code. This work was supported by the National Science Foundation, through the Network for Computational Nanotechnology at Purdue, and the NSF-DMR program through the Northwestern University Materials Research Science and Engineering Center.

[1] E. J. Bjerneld, K. V. G. K. Murty, J. Prikulis, and M. Kall, ChemPhysChem **3**, 116 (2002).
[2] E. J. Bjerneld, F. Svedberg, and M. Kall, Nano Lett. **3**, 593 (2003).
[3] C. L. Asbury, A. N. Fehr, and S. M. Block, Science **302**, 2130 (2003).
[4] M. M. Wang, E. Tu, D. E. Raymond, J. M. Yang, H. C. Zhang, N. Hagen, B. Dees, E. M. Mercer, A. H. Forster, I. Kariv, P. J. Marchand, and W. F. Butler, Nat. Biotechnol. **23**, 83 (2005).
[5] J. R. Arias-Gonzalez, M. Nieto-Vesperinas, and M. Lester, Phys. Rev. B **65**, 115402 (2002).
[6] P. C. Chaumet, A. Rahmani, and M. Nieto-Vesperinas, Phys. Rev. B **71**, 045425 (2005).
[7] H. Xu and M. Kall, Phys. Rev. Lett. **89**, 246802 (2002).
[8] J. Prikulis, F. Svedberg, M. Kall, J. Enger, K. Ramser, M. Goksor, and D. Hanstorp, Nano Lett. **4**, 115 (2004).
[9] A. J. Hallock, P. L. Redmond, and L. E. Brus, Proc. Natl. Acad. Sci. U.S.A. **102**, 1280 (2005).
[10] K. Svoboda and S. M. Block, Opt. Lett. **19**, 930 (1994).
[11] L. Novotny, R. X. Bian, and X. S. Xie, Phys. Rev. Lett. **79**, 645 (1997).
[12] P. C. Chaumet and M. Nieto-Vesperinas, Phys. Rev. B **64**, 035422 (2001).
[13] L. Novotny, Top. Appl. Phys. **81**, 123 (2001).
[14] V. Wong and M. A. Ratner (unpublished).
[15] J. R. Arias-Gonzalez and M. Nieto-Vesperinas, J. Opt. Soc. Am. A **20**, 1201 (2003).
[16] M. Nieto-Vesperinas, P. C. Chaumet, and A. Rahmani, Philos. Trans. R. Soc. London, Ser. A **362**, 719 (2004).
[17] V. Wong and M. A. Ratner (unpublished).
[18] A. Ashkin and J. P. Gordon Opt. Lett. **8**, 511 (1983).
[19] P. C. Chaumet and M. Nieto-Vesperinas, Opt. Lett. **25**, 1065 (2000).
[20] J. P. Gordon and A. Ashkin, Phys. Rev. A **21**, 1606 (1980).
[21] P. C. Chaumet and M. Nieto-Vesperinas, Phys. Rev. B **62**, 11185 (2000).
[22] G. E. Hay, *Vector and Tensor Analysis* (Dover, New York, 1953).
[23] B. T. Draine, Astrophys. J. **333**, 848 (1988).
[24] B. T. Draine and P. J. Flatau, *User guide to the discrete dipole approximation code* DDSCAT 6.0 (2003), astro-ph/0309069.
[25] A. G. Hoekstra, M. Frijlink, L. B. F. M. Waters, and P. M. A. Sloot, J. Opt. Soc. Am. A **18**, 1944 (2001).
[26] R. Jin, Y. C. Cao, E. Hao, G. S. Metraux, G. C. Schatz, and C. A. Mirkin, Nature (London) **425**, 487 (2003).
[27] M. Maillard, P. Huang, and L. Brus, Nano Lett. **3**, 1611 (2003).
[28] A. Callegari, D. Tonti, and M. Chergui, Nano Lett. **3**, 1565 (2003).
[29] W. A. Kraus and G. C. Schatz, J. Chem. Phys. **79**, 6130 (1983).
[30] R. Fuchs and F. Claro, Phys. Rev. B **35**, 3722 (1987).
[31] S. D. Druger and B. V. Bronk, J. Opt. Soc. Am. B **16**, 2239 (1999).
[32] A. Rahmani, P. C. Chaumet, and G. W. Bryant, Astrophys. J. **607**, 873 (2004).
[33] M. J. Collinge and B. T. Draine, J. Opt. Soc. Am. A **21**, 2023 (2004).